



# Particle size distribution of aggregates effects on mesoscopic structural evolution of cemented waste rock backfill

Jiangyu Wu<sup>1</sup> · Qian Yin<sup>1</sup> · Yuan Gao<sup>1</sup> · Bo Meng<sup>2</sup> · Hongwen Jing<sup>1</sup>

Received: 17 September 2020 / Accepted: 19 November 2020 / Published online: 2 January 2021  
© Springer-Verlag GmbH Germany, part of Springer Nature 2021

## Abstract

The most economical, environmental, and friendly method for recycling gangue is filling mining with cemented waste rock backfill (CWRB), which solves the environmental problems caused by gangue discharge and reduces the mining damages. Evaluating the mesoscopic structure of CWRB is of great significance for maximizing the utilization of gangue recycling and improving the economic benefits of filling mining. This paper constructed the particle flow model of cemented waste rock backfill (CWRB) considering particle size distribution (PSD) of aggregates and hydration of cementing material to investigate the effect of the PSD of aggregates on its mesoscopic structural evolution. The strain energy, crack, force chain, and particle fragment of CWRB during the whole loading were discussed. The binary processing and calculation on the crack image were performed to analyze the fractal dimension of crack distribution by compiling program. The influencing mechanism of the PSD of aggregates on the strength of CWRB is revealed from the mesoscopic levels of crack evolution, force chain structure, and particle fragment. The results show that the strain energy increases firstly and then decreases with the PSD fractal dimension, while the crack number decreases firstly and then increases with that. The cracks with less number and more uniform distribution present the smaller fractal dimension, CWRB with a low fractal dimension of crack distribution has higher strength, the fractal dimension of crack distribution exhibits a correlation with the PSD of aggregates. CWRBs with the PSD fractal dimensions of 2.4–2.6 have the largest strain energy and the smallest crack number, performing the superior structural evolution during loading. This study presents the huge potential of optimizing PSD in CWRB application from a new perspective, it is of great significance for strengthening the internal structure of CWRB and reducing engineering cost.

**Keywords** Cemented waste rock backfill · Particle size distribution · Mesoscopic structural evolution · Particle flow simulation · Fractal dimension

## List of symbols

CWRB Cemented waste rock backfill

$d_i$  Size of aggregate particles

$d_{\max}$  Maximum size of aggregate particles

Responsible editor: Philippe Garrigues

✉ Qian Yin  
jeryin@foxmail.com

✉ Hongwen Jing  
hwjingcumt@126.com

<sup>1</sup> State Key Laboratory for Geomechanics and Deep Underground Engineering, China University of Mining and Technology, Xuzhou 221116, Jiangsu, China

<sup>2</sup> School of Mechanics and Civil Engineering, China University of Mining and Technology, Xuzhou 221116, Jiangsu, China

$D$	PSD fractal dimension
$D_c$	Fractal dimension of crack distribution
$M_i$	Mass of aggregate particles in size below or equal to $d$ , $M_i = M_t \left( \frac{d_i}{d_{\max}} \right)^{3-D}$
$M_t$	Total mass of aggregate particles
$N_i$	Crack number
$N_b$	Box count
$N_c$	Cumulative crack number
$N_t$	Total boxes
$P_i$	Mass ratio of aggregate particles, $P_i = \frac{M_i}{M_t} = \left( \frac{d_i}{d_{\max}} \right)^{3-D}$
PSD	Particle size distribution
$U$	Strain energy
SEM	Scanning electron microscope
UCS	Uniaxial compressive strength
XRD	X-ray diffraction

$\sigma_1$	Axial stress
$\sigma_{1c}$	Peak stress, $\sigma_{1c} = \text{UCS}$
$\varepsilon$	Axial strain
$\varepsilon_{1c}$	Peak strain

## Introduction

Gangue produced by coal mining causes environmental pollution, releasing harmful elements to the air and water resources (Li et al. 2020). A large amount of gangue accumulates to form the waste mountains occupying land, which seriously damage sustainable development (Li et al. 2017). Especially in the development of coal resources under buildings, railways, and waters, the problem of coordination between human and nature is particularly severe (Bian et al. 2012; Ma et al. 2021). In China, more than 4.5 billion tons of gangue accumulated about 1600 waste mountains, it is urgent to recycle gangue (Ma et al. 2019a). The most economical, environmental, and friendly method is to use the gangue as the aggregate of cemented waste rock backfill (CWRB) to filling mining.

The structural stability of CWRB under the action of surrounding rock pressure is the key to ensure the stope safety (Cao et al. 2018; Shi and Zhao 2020). If its structure fails, it will cause the underground dynamic disaster, groundwater loss, and destruction of surface structures (Cao et al. 2021; Liu et al. 2018; Ma et al. 2019b, 2020). Most of the previous studies focused on the influence of cementing materials and auxiliary additives on the strength property of CWRB (Benzaazoua et al. 2002; Cao et al. 2019; Cui and Fall 2016). It is believed that the key to the strength of CWRB is the hydration products that constitute its loading structure. The internal structure of CWRB was directly or indirectly investigated from the point by optimizing the hydration process or hydration products (Deng et al. 2017; Yilmaz et al. 2015). However, the types and dosages of cementing materials and auxiliary materials are always restricted by engineering conditions and economic benefits (Cihangir et al. 2012; Ercikdi et al. 2009a; Wu et al. 2016; Yilmaz 2018). The cost of cementing materials that can be used for backfill mining is usually limited, which enforces us to explore ways to improve the structure of CWRB from other directions (Chen et al. 2018; Ercikdi et al. 2009b; Wu et al. 2020). The particle size distribution (PSD) of high mass fraction aggregates in CWRB determines whether the pores among the coarse aggregates inside can be fully filled with fine aggregates and slurries, whether the hydration products and aggregates with a more suitable PSD can form a more stable framework structure (Ercikdi et al. 2014; Sari and Pasamehmetoglu 2005). The differences in aggregate particle size spans, multiplicities of aggregate mass distributions, and various test conditions cause lots of entirely different research results in the current (Fall et al. 2005; Jiang et al. 2020). There is still no consensus on

the relationship between structural parameters of CWRB and its PSD of aggregates, the influencing mechanism of PSD on the backfill structure is so vague (Ke et al. 2016; Wu et al. 2019). The root is the understanding lack of the internal structure of CWRB, especially for its structural evolution under deformation during loading (Sun et al. 2019). The difference in the damage of structural evolution inevitably affects the performance of CWRB. It is so difficult to capture the structural evolution of CWRB in the whole experimental process in real-time, the damage and fracture of the weak cementing boundary in framework structure and the propagation and coalescence of the crack in pore structure are not identified by existing test technology (Wu et al. 2018). At present, the simulation study on the mesoscopic structural evolution of CWRB was not considered the difference in PSD of high mass fraction aggregates (Liu et al. 2017). Moreover, most studies still use a single mesoscopic contact model to describe the internal particles of CWRB; there is no distinction between the frictional slip of the aggregate particles and the bond fracture of the cementing particles (Liu et al. 2020), thereby revealing the control mechanism of optimizing PSD on the structure of CWRB from the level of mesoscopic structural evolution impossible.

In this paper, the particle flow model of CWRB considering the PSD of aggregates and hydration of cementing material was constructed. The effects of the PSD of aggregates on the strain energy, crack, force chain, and particle fragment of CWRB during the whole loading were investigated. The binary processing and calculation on the crack image were performed to obtain the fractal dimension of crack distribution by compiling the program. The influencing mechanism of the PSD of aggregates on the structure and strength of CWRB is revealed from the mesoscopic levels of crack evolution, force chain structure, and particle fragment. This research is a pioneering work that presents the huge potential of optimizing PSD in CWRB application from a new perspective, it is of great significance for strengthening the internal structure of CWRB and reducing engineering cost.

## Materials and methods

### Experimental materials

The physical and chemical properties of aggregates and cementing materials determine the processability of CWRB. In this test, the gangue with a density of  $2.55 \text{ g/cm}^3$  was used as the aggregates, the composite Portland cement (PCC 32.5R) was used as the cementing materials, Table 1 gave their main chemical compositions. The gangue containing silica at 67.75% has enough matrix strength as aggregates, the cement with Ca/Si of 4.4:1 ensures abundant hydration products to provide sufficient strength.

**Table 1** Chemical compositions of experimental materials

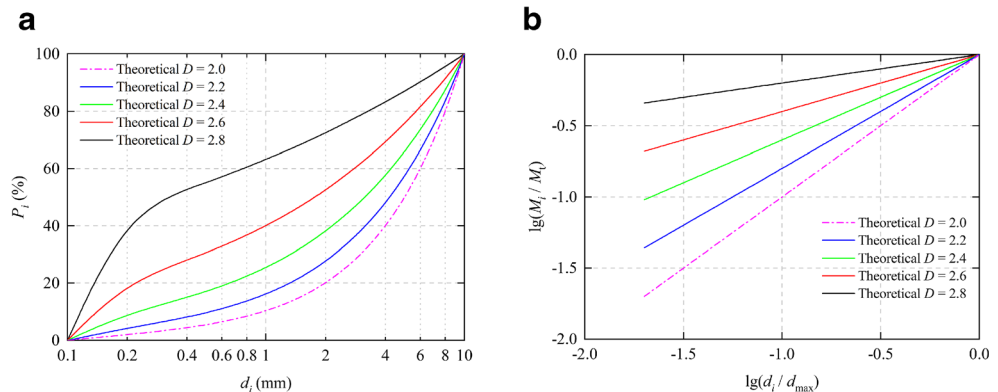
Compound	Cement (%)	Gangue (%)
Al <sub>2</sub> O <sub>3</sub>	4.67	13.21
CaO	62.19	3.91
Fe <sub>2</sub> O <sub>3</sub>	3.69	5.27
K <sub>2</sub> O	0.68	0.02
MgO	2.87	2.87
Na <sub>2</sub> O	0.21	–
SiO <sub>2</sub>	21.56	67.75
SO <sub>3</sub>	1.91	–
TiO <sub>2</sub>	0.16	–

**Preparations of CWRB specimens**

The material design parameters of CWRB such as PSD of aggregates, dosage of cementing material, and water-cement ratio determine its processability, which affects engineering economy and filling efficiency. In this study, CWRB is mainly used for the filling mining of coal resources under three of buildings, railways, and waters, so its cement mass percentage at 14.8% is higher than previous situations, its water/cement ratio is 0.75. This test focuses on the effect of the PSD of aggregates on the structure of CWRB to optimize the PSD of gangue in filling mining. The maximum particle size of aggregate is determined as 10 mm to eliminate the size effect for a standard cylindrical specimen in size of  $\phi 50 \times 100$  mm with a ratio of height to diameter at 2:1 (ASTM 2013). The PSD of aggregates in CWRB satisfies the formula (1), the fractal dimension is used to describe the PSD. Figure 1 shows the PSD of gangue aggregates used in this test and its corresponding fractal dimension. It can be seen from Fig. 1 that the larger the PSD fractal dimension, the more fine particles are contained in the aggregates, while the aggregates with smaller PSD fractal dimension have the more coarse particles.

$$P_i = \frac{M_i}{M_t} = \left( \frac{d_i}{d_{max}} \right)^{3-D} \tag{1}$$

**Fig. 1** PSD of gangue aggregates in CWRB



$$D = 3 - \frac{\lg(M_i/M_t)}{\lg(d_i/d_{max})} \tag{2}$$

where  $P_i$  is the ratio of the mass  $M_i$  of the aggregate particles having a particle size of less than or equal to  $d_i$  to the total mass  $M_t$ ,  $d_{max}$  is the maximum particle size of the aggregate particles,  $D$  is the PSD fractal dimension.

Table 2 gives the preparation program of CWRB, in which the percentage is the mass ratio. The cement and water were mixed for 10 min; the prepared aggregates with different PSDs were stirred with this slurry for 10 min to produce the CWRB specimen (Zuo et al. 2018). After finally setting, the CWRB specimen was placed in a curing box maintained at 95% humidity and 25 °C for 84 days (Belem and Benzaazoua 2008).

**Experimental devices**

The uniaxial compression test of CWRB was carried out on the MTS815 electrohydraulic servo-controlled rock mechanics test system (ASTM 2015). The circumferential extensometer was connected to the middle of the specimen, the prestress on the specimen was set to 0.25 kN, the rate of 1 mm/min was used to load. The MTS system automatically records the axial stress, axial strain, circumferential strain, and volumetric strain.

**Particle flow model of CWRB**

CWRB is a porous medium formed by hydration products and aggregates. The construction of its particle flow model must take into account the differences in its internal components and PSD of aggregates. So the QuantaTM 250 from FEI Corporation in USA was used to conduct the scanning electron microscope (SEM) test on CWRB to illustrate its microstructure. Figure 2 shows the microscopic characteristics of CWRB with a PSD fractal dimension of aggregates of 2.6, Fig. 2a presents  $\times 100$  magnifications, Fig. 2b reveals  $\times 4000$  magnifications. The aggregates encapsulated by the

**Table 2** Preparation program of CWRB specimen

D	Cement/CWRB (%)	Aggregate/CWRB (%)	Water/Cement (%)
2.2	14.8	74.1	75
2.4	14.8	74.1	75
2.6	14.8	74.1	75
2.8	14.8	74.1	75

hydration products can be seen in Fig. 2a. The cementing material reacts with water to produce various hydration products, including ettringite, calcium silicate hydrate (C-S-H), and calcium hydroxide, as presented in Fig. 2b. It is difficult to distinguish these complex hydration products in the numerical model, so the particles with bonding property are used to characterize the hydration products uniformly; its density and volume satisfy the cement slurry parameters. Bulk aggregate does not have bonding property, but it can still load by friction and slippage. Its density, volume, and PSD obey the actual parameters of gangue, as shown in Fig. 3a. Then a “two media - three boundaries” mesoscopic model was established to describe two components (hydration products and aggregates) and three boundaries (aggregate-aggregate, aggregate-cement, and cement-cement), as illustrated in Fig. 3b. It is believed that only in the existence of cementing particles did it have cementing property; the aggregate-aggregate behavior is only friction and slippage. Too many particles are not conducive to calculate particle flow model of CWRB, but the fact that the cementing slurry fully packs the aggregate should be satisfied. So the cementing particles are uniformly generated within the size range of 0.05 and 0.2 mm, the corresponding PSD fractal dimension is 2. The aggregate particles are generated according to the formula (1) within the size range of 0.4 and 10 mm, the corresponding PSD fractal dimension is consistent with the test, as given in Fig. 4.

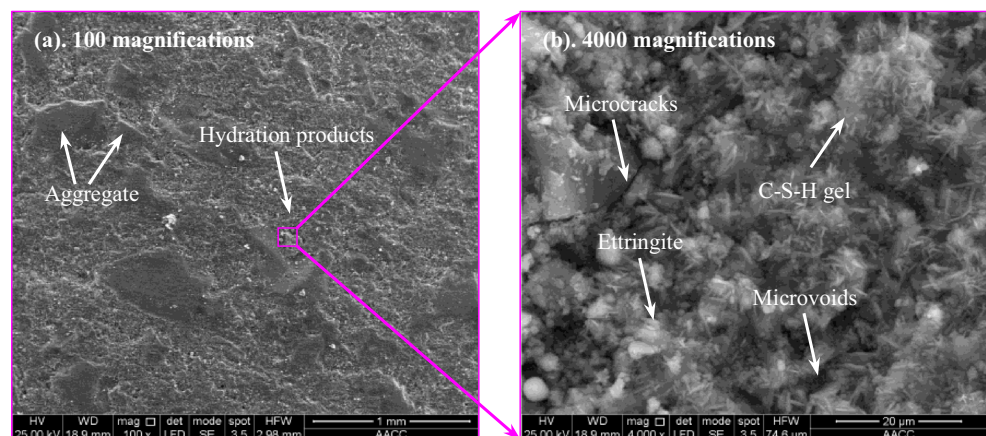
In the uniaxial compression test, the experimental system compresses the specimen at a quasi-static loading rate of 0.1 mm/min. To match the model to the experiment, the

loading plate loads the specimen at a constant rate of 0.05 m/s in the particle flow program, the time step of the model is about  $1.3\text{--}1.6 \times 10^{-8}$  s to ensure that the specimen maintains quasi-static equilibrium throughout the compression. It means that loading a specimen of 1 mm in the model requires performing a numerical calculation at  $1.25\text{--}1.55 \times 10^6$  steps. According to the calibration method of mesoscopic parameters (Huang et al. 2019; Tian et al. 2020), the axial stress-axial strain, compressive strength, and peak strain of CWRB are matched with the experimental results, Table 3 and Table 4 give the particle parameters and mesoscopic parameters of the particle flow model.

## Results and discussions

### Simulation verification

The “two media - three boundaries” mesoscopic model and particle flow model of CWRB considering PSD of aggregates need to be verified to investigate the match between numerical simulation and experiment. Figures 5 and 6 show the difference between simulation and experiment in stress-strain behavior, uniaxial compressive strength (UCS), and peak strain of CWRB. In terms of UCS, peak strain and stress-strain behavior before the peak, the simulation is almost consistent with the experiment. The stress-strain behavior after the peak shows a certain difference between simulation and experiment. In the particle flow model, due to the application of circular particle elements and parallel bonding model, the bonding particles fracture and slip, resulting in the stress dropping. In the experiment, CWRB performs a certain residual strength and ductility after the peak caused by the framework composed of hydration products and interlaced aggregates. In this paper, the focus is on the mesoscopic structural evolution of CWRB before the peak; the consistency of the simulation and experiment indicates the reliability of the constructed model.

**Fig. 2** Microstructure of CWRB

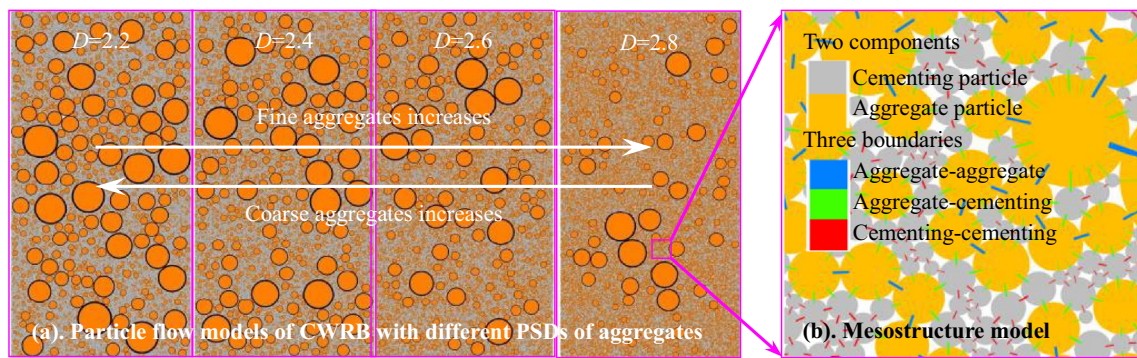


Fig. 3 Particle flow model of CWRB

**Crack and energy evolution**

Figure 7 shows the effect of the PSD of aggregates on the stress, strain energy, and crack evolution of CWRB throughout the compression. The strain energy and crack increase with the stress, but the increase in stress does not completely translate into the strain energy stored in CWRB. All the pore compaction, particle fracture and crack initiation in CWRB have energy dissipation, so the variation of strain energy present nonlinear. The peak stress basically corresponds to the peak strain energy. When the stress drops, the stored strain energy is also suddenly released, thereby generating a large number of tensile and shear cracks. It should be noted that the CWRBs with PSD fractal dimensions of 2.2 and 2.8 produce cracks earlier than those of 2.4 and 2.6, they showed a denser crack propagation during loading. This indicates that the PSD of aggregates affects the crack development of CWRB during loading to transform its internal structure evolution, the worse PSD causes the early crack initiation and the accumulation of crack development.

It is easy to find in Fig. 6 that the UCS of CWRB basically has a quadratic polynomial relationship with the PSD fractal dimension, indicating that a superior PSD of aggregates can improve the strength of CWRB. However, the single strength index does not reflect the deformation performance of

CWRB, so the energy feedback of CWRB under the action of goaf roof should pay more attention. Figure 8 reveals the effect of the PSD of aggregates on the strain energy and crack number of CWRB at the peak point. The strain energy increases firstly and then decreases with the PSD fractal dimension, while the crack number decreases firstly and then increases with that. The CWRBs with the PSD fractal dimensions of 2.4 to 2.6 show the largest strain energy and the smallest crack number. It proves that the CWRB with a superior PSD of aggregates performs less damage during loading; it can also store more strain energy, meaning that the CWRB having optimal PSD of aggregates can absorb more energy released by the roof.

The distribution of initiating cracks affects the mesoscopic structural evolution of CWRB; even small local crack accumulation can lead to the failure of the entire structure; these crack distributions are affected by the PSD of aggregates. Figure 9 exposes the crack distribution of CWRB under different stress states, of which the 100% is at the peak stress, the 40%, 60%, and 80% are the percentages of strength before the peak, the 120% is the point that the stress drops 20% after the peak. The CWRB with a PSD fractal dimension of 2.8 has a low mass fraction of coarse aggregates and contains too many fine aggregates, which results in a weak framework structure. The upper left part of the structure reveals a weak framework effect; a large number of cracks initiate at the bonding boundary of fine aggregates and hydration products; the coalescence of local tensile and shear cracks cause the failure of the entire structure. The lower part of the structure containing coarse aggregates presents a certain framework

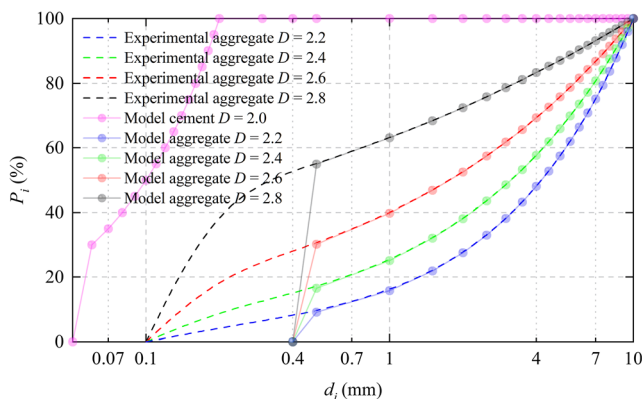


Fig. 4 Cumulative PSD curve of aggregates and cementing particles in model of CWRB

Table 3 Particle parameters of CWRB particle flow model

D	Aggregate particles	Cementing particles	Total particles	Balance steps
2.2	2500	29,677	32,177	50,318
2.4	4029	29,644	33,673	17,006
2.6	6614	29,631	36,245	22,004
2.8	10,048	29,694	39,742	12,348

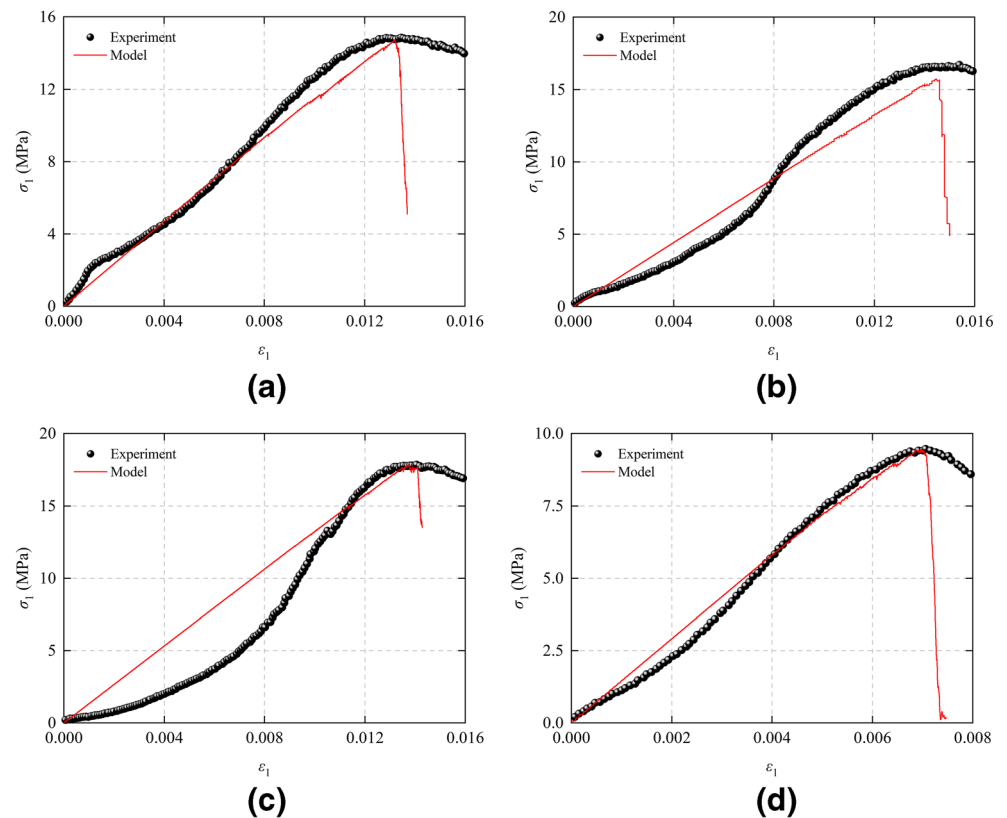
**Table 4** Mesoscopic parameters of CWRB particle flow model

Boundary	Aggregate-aggregate	Aggregate-cementing	Cementing-cementing
Effective modulus (GPa)	9.0	1.5	3.6
Normal-to-shear stiffness ratio	3.0	1.25	1.0
Tensile strength (MPa)	–	20	35
Cohesion (MPa)	–	12.5	30
Friction angle (°)	–	25	30
Friction coefficient	–	0.75	0.65

effect; the initiation of the tensile and shear cracks is less than that of the upper left part. In the CWRB with a PSD fractal dimension of 2.2, the mesoscopic structure formed by a large number of coarse aggregates and hydration products seems to exhibit a strong framework effect, but some large pores occur among the coarse aggregates that the slurry cannot be completely filled. The cracks are more likely to initiate at the tip of such large pores to accumulate, thereby coalescing the framework structure, which is so unfavorable for CWRB. In contrast, the CWRB with PSD fractal dimensions of 2.4 and 2.6 does not present such severe mesoscopic structural deterioration, but it also performs the local crack accumulation to induce the structural instability in a certain extent. This certifies the benefits of finding the optimal PSD of aggregates for CWRB. Assi et al. (2018) also indicated that the PSD could affect the crack distribution in the material,

which in turn caused the differences in its strength and structure through scanning electron microscope (SEM) tests. However, the difference between Assi et al. (2018) and this study is that the crack distribution is not the initial condition of the material under static conditions. The dynamic crack evolution of the material under loading is illustrated in this paper. Since the essence of the deformation and failure of material is the damage evolution of its internal structure, the influencing mechanism of the PSD of aggregates on the strength of CWRB is revealed from the difference in the crack evolution, which provides a new perspective in the current research.

To quantify the effect of the PSD of aggregates on the crack distribution of CWRB, the fractal dimension  $D_c$  is used to describe the crack distribution in its structure. In this study, the box counting method was improved to calculate the fractal dimension of crack distribution. The original image was

**Fig. 5** Verification of stress-strain behavior

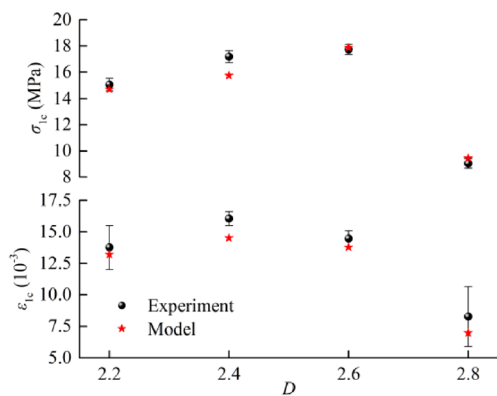


Fig. 6 Verification of peak parameters

transformed into a monochrome image as shown in Fig. 10a, then a binary image was obtained in Fig. 10b based on the adaptive grayscale threshold. Figure 10 gives the example having a length of 760 pixels and a width of 760 pixels, the value of each pixel is 1 or 0. The image was covered by a square frame ranging in size from  $760 \times 760$  pixels (1 frame) to  $1 \times 1$  pixel ( $760 \times 760$  frames). If the pixels in the box are not empty, the value of the box is 1, otherwise it is 0. A logarithmic figure of the box count  $N_b$  and the total boxes  $N_t$  is plotted in Fig. 10c, the slope represents the fractal dimension. The calculated results

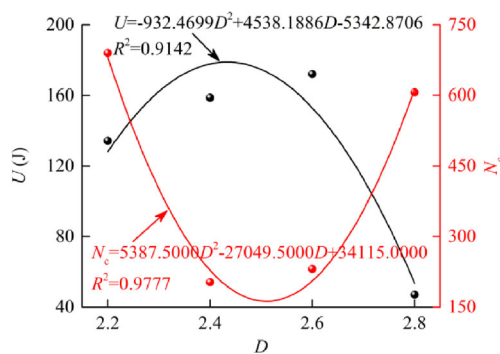


Fig. 8 Relation between PSD of aggregates and energy and crack at peak point

are compared with the theoretical values, the deviation between both is less than 0.5%. Therefore, this program is considered to reliably estimate the fractal dimension.

Figure 11 shows the effect of the PSD of aggregates on the fractal dimension of crack distribution at the peak stress of CWRB. The increase in the crack number leads to an increase in the fractal dimension of crack distribution, but it depends more on the crack distribution. The crack number of CWRB with a PSD fractal dimension of 2.8 has reached 3 times that of 2.6, but the difference in both fractal dimensions is only 0.001.

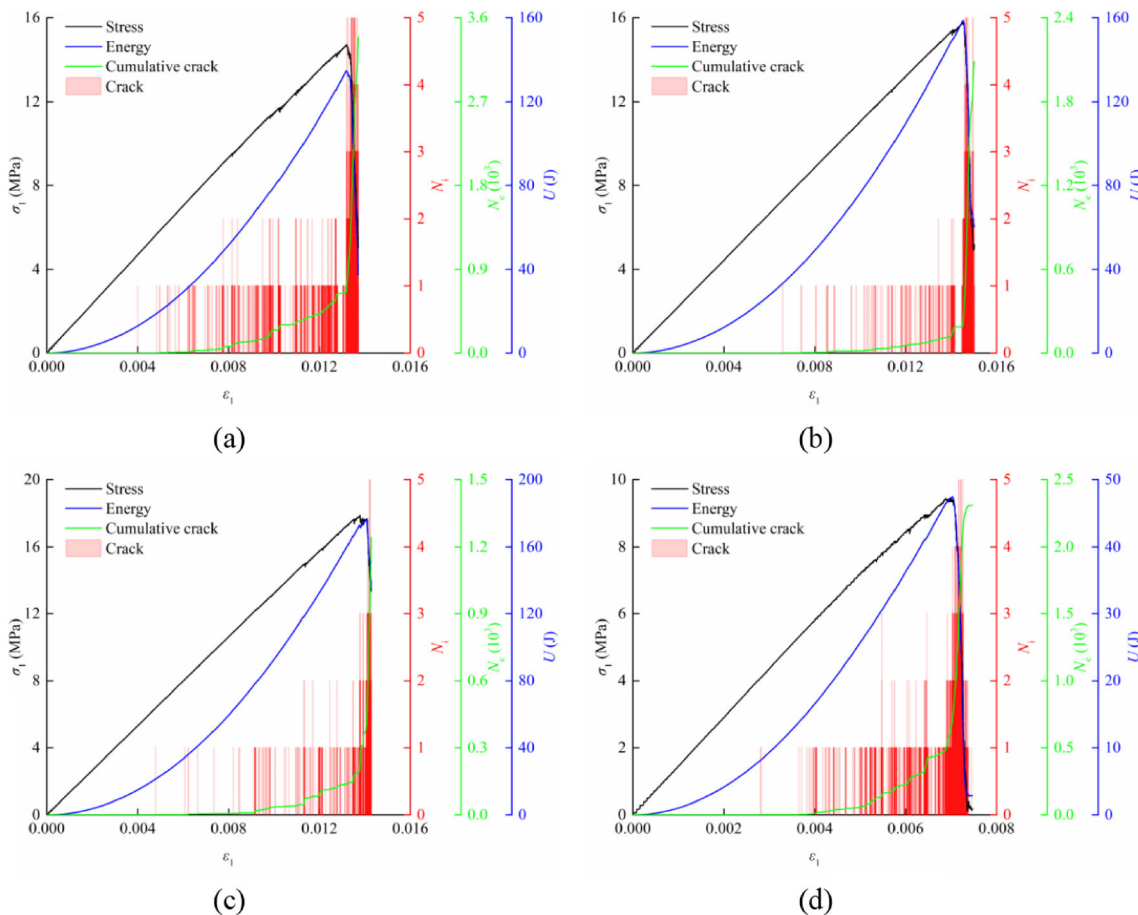
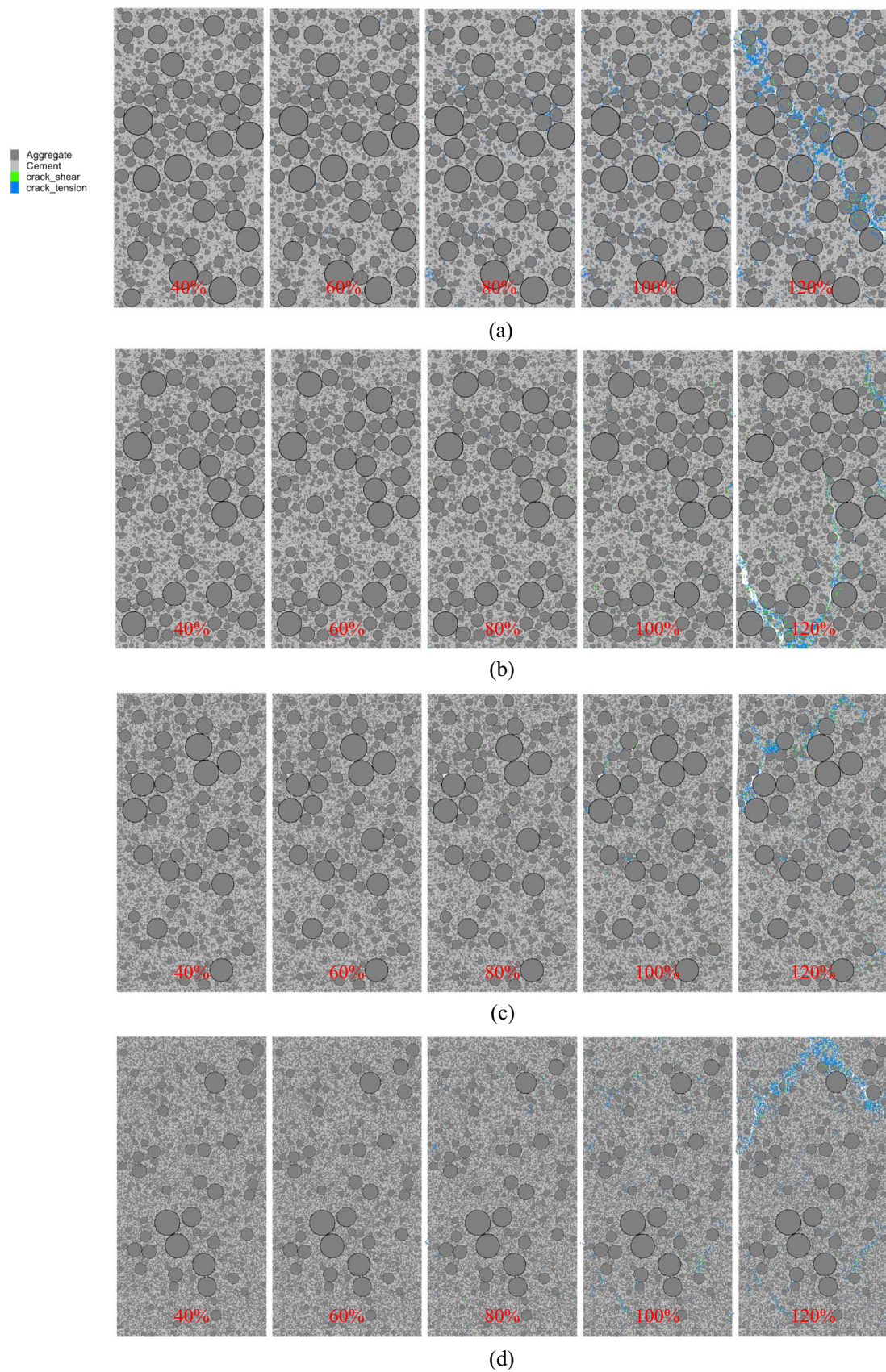


Fig. 7 Stress-energy-crack evolution of CWRB



**Fig. 9** Crack evolution of CWRB



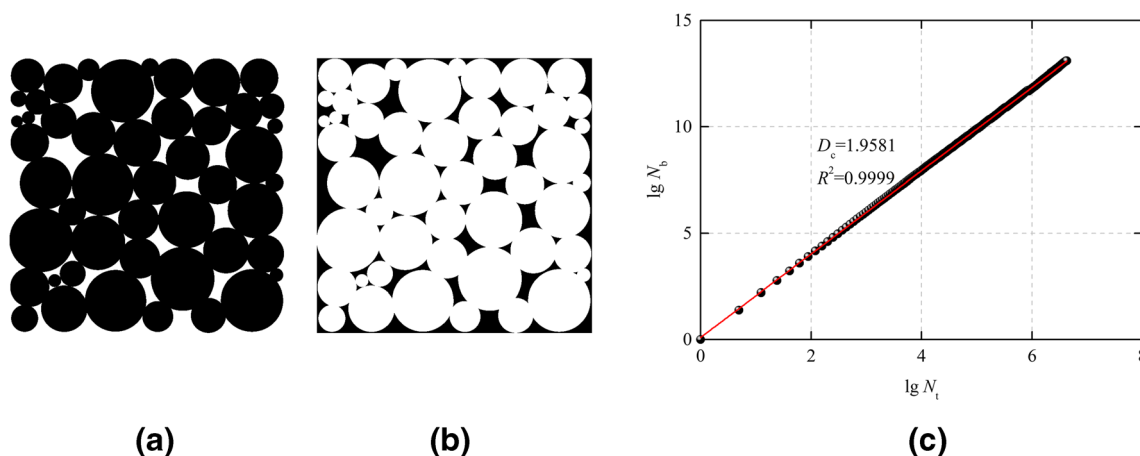


Fig. 10 Image processing and fractal dimension of crack distribution

The crack number of CWRB with a PSD fractal dimension of 2.6 is not much different from that of 2.4 as shown in Fig. 8, while the fractal dimension is different by 0.103. The reason for this is that the CWRB with a PSD fractal dimension of 2.6 has crack accumulation in the upper left and middle parts of the structure, while the crack distribution of the CWRB with a PSD fractal dimension of 2.4 is more uniform. The CWRB with a PSD fractal dimension of 2.2 has the largest number of cracks and crack accumulations in multiple locations, so its fractal dimension of crack distribution is the largest. The UCS of CWRB given in Fig. 8 can also be found that the CWRB with a lower fractal dimension of crack distribution has higher strength. It can be seen that the fractal dimension of crack distribution is applicative for evaluating the mesoscopic structure of CWRB. However, this fractal dimension crack distribution does not seem to describe the framework effect of CWRB during loading. For example, the fractal dimension of crack distribution in CWRB with a PSD fractal dimension of 2.2 is the largest, but its UCS is not the lowest, which is higher than the CWRB with a PSD fractal dimension of 2.8.

This can be understood that the low mass fraction of coarse aggregates of CWRB with a PSD fractal dimension of 2.8 weakens its framework structure.

### Force chain structure

The force chain structure can reflect the framework effect of CWRB performing by the combinations of hydration products and different aggregates with different PSDs. Figure 12 presents the force chain structure of CWRB under different stress states. The PSDs of aggregates conduct a small effect on the force chain structure of CWRB before the peak stress; it only performs the difference in the force chain value. It can be observed that the strength of the force chain of CWRB with a PSD fractal dimension of 2.6 is the highest. The effect of the PSD of aggregates on the force chain structure of CWRB began to emerge near the peak stress. The force chain structures of CWRBs with the PSD fractal dimensions of 2.4 and 2.6 are more uniform, while the CWRBs with the PSD fractal dimensions of 2.8 and 2.2 exhibit a weak force chain structure, the fractures of the local force

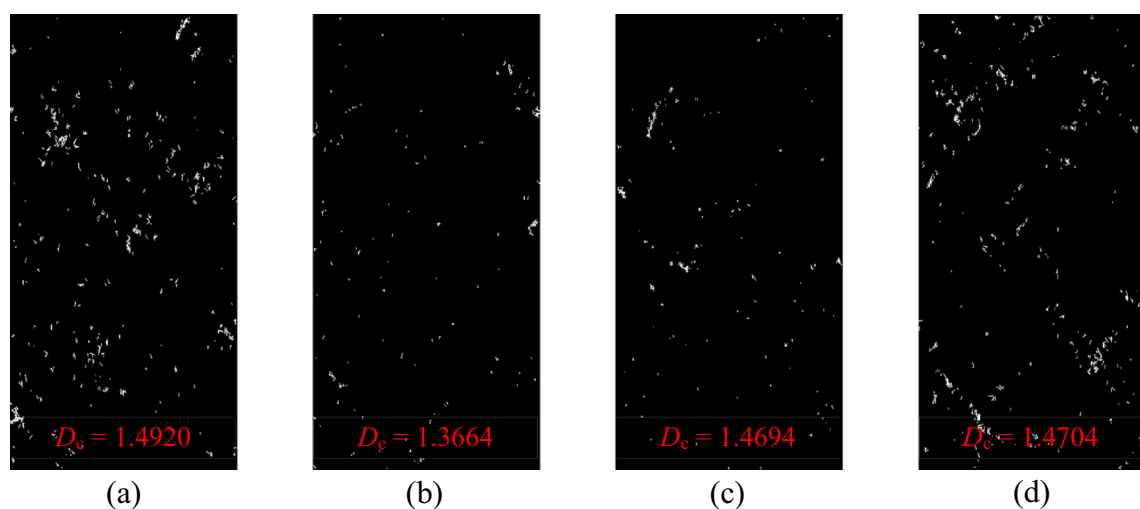


Fig. 11 PSD of aggregates effects on fractal dimension of crack distribution

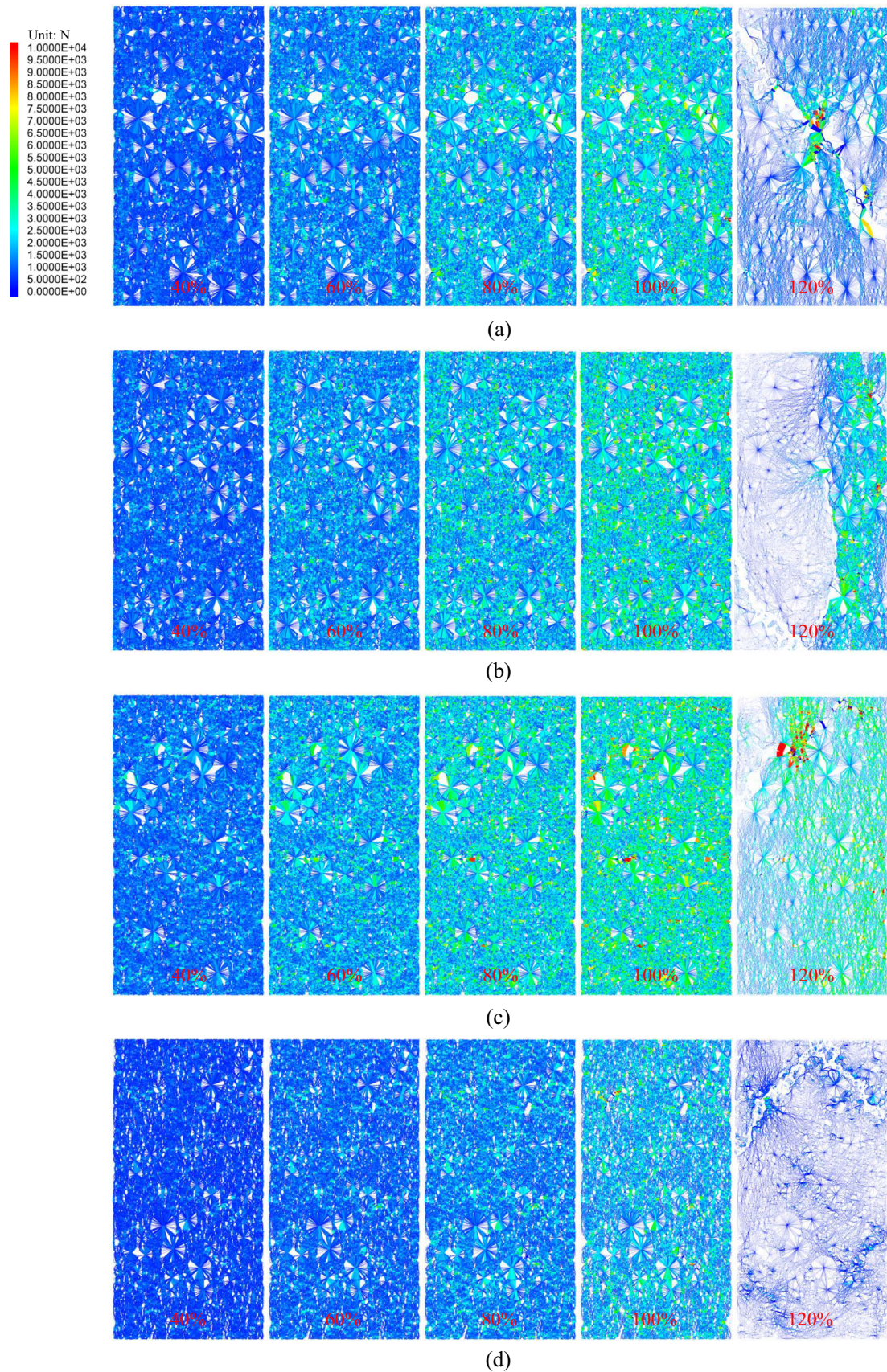


Fig. 12 Force chain structure of CWRB

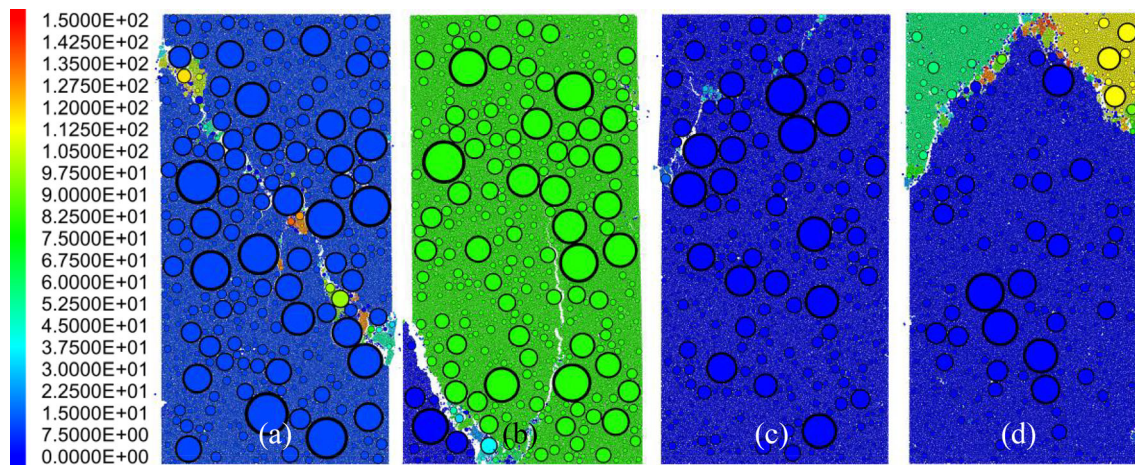


Fig. 13 Particle fragment of CWRB

chains deteriorate the framework structure. This characteristic is more obvious after the peak stress. The CWRB with a PSD fractal dimension of 2.8 only depends on the local framework at the upper left and lower right parts to load; a small local framework at the middle part formed by the hydration products and coarse aggregates has the loading capacity for the CWRB with a PSD fractal dimension of 2.2. The opposite is that the force chain structures of CWRBs with the PSD fractal dimensions of 2.4 and 2.6 present a stronger and wider framework. This is consistent with the results of Sevim and Demir (2019). They indicated that the strength of the material also increases firstly and then decreases with the distribution parameter of the Funk gradation; there was a maximum strength in the middle of the gradation range. Wu et al. (2020) proved that this moderate PSD of aggregates has the superior microstructure for CWRB through the SEM test. However, this traditional method for evaluating the microstructure of the material by analyzing the initial structure cannot reflect the structural evolution of CWRB under the whole loading process, it is limited to a small range of microscopic observations that cannot describe the entire structure, thereby causing the indistinction in the influencing mechanism of the PSD of aggregates on the strength of CWRB. The particle flow simulation was consequently used to reproduce the mesoscopic structural evolution of CWRB in the current study. The results show that the CWRBs with different PSDs of aggregates perform the various framework effects through affecting its internal force chain structures, thereby resulting in the differences in strength parameters.

### Particle fragment

Figure 13 gives the particle fragments of CWRBs with different PSDs of aggregates, the greater value represents the more serious damage to the particles. The failure degrees of CWRBs with the PSD fractal dimensions of 2.4 and 2.6 are lower than those of 2.2 and 2.8. Due to the defect in the PSD of aggregates, all CWRBs inevitably have structural

instabilities induced by local damages. The partial destruction of CWRB with a PSD fractal dimension of 2.8 is caused by the lack of a framework structure formed by hydration products and interlaced coarse aggregates. The large pores that are not fully filled by the slurry lead to the coalescence failure of the framework structure of CWRB with a PSD fractal dimension of 2.2. From the mesoscopic level of particle fragment, a superior PSD of aggregates can effectively weaken the deterioration of CWRB. This indicates that the optimization of the PSD of aggregates has unprecedented potential for improving the structure and strength of CWRB. In the future study, the comprehensive consideration of the crack evolution, force chain structure, and particle fragment of CWRB under loading is the key to exploring the optimal PSD of aggregates. This improvement of the mesoscopic structure can fully illustrate the optimization mechanism of the PSD of aggregates to CWRB. Although this method is time-consuming and laborious, it is expected to break through the limitations of existing evaluation methods. It certainly needs to further improve its theory; the shape of the aggregates and the difference in pore structure caused by different PSDs based on this work should be considered for perfecting this method.

### Conclusions

In this paper, the particle flow model of CWRB considering the PSD of aggregates and hydration of cementing material was constructed. The effects of the PSD of aggregates on the strain energy, crack, force chain, and particle fragment of CWRB during the whole loading were investigated. The binary processing and calculation on the crack image were performed to obtain the fractal dimension of crack distribution by compiling the program. The influencing mechanism of the PSD of aggregates on the structure and strength of CWRB is revealed from the mesoscopic levels of crack evolution, force chain structure, and particle fragment.

The results show that the strain energy increases firstly and then decreases with the PSD fractal dimension, while the crack number decreases firstly and then increases with that. The CWRBs with the PSD fractal dimensions of 2.4 to 2.6 show the largest strain energy and the smallest crack number. It proves that the CWRB with a superior PSD of aggregates performs less damage during loading, it can also store more strain energy, which means that the CWRB having optimal PSD of aggregates can absorb more energy released by the roof. The CWRBs with different PSDs of aggregates perform the various framework effects through affecting its internal force chain structures, thereby resulting in the differences in strength parameters. The CWRB with a PSD fractal dimension of 2.8 has a low mass fraction of coarse aggregates and contains too many fine aggregates, which results in a weak framework structure, the coalescence of local tensile and shear cracks cause the failure of the entire structure. In the CWRB with a PSD fractal dimension of 2.2, the mesoscopic structure formed by a large number of coarse aggregates and hydration products seems to exhibit a strong framework effect, but some large pores occur among the coarse aggregates that the slurry cannot be completely filled. The local damage is caused by these large pores, which result in the coalescence of the framework structure. The cracks with less number and more uniform distribution present the smaller fractal dimension; the CWRB with a low fractal dimension of crack distribution has higher strength; the fractal dimension of crack distribution exhibits a certain correlation with PSD of aggregates. The CWRBs with the PSD fractal dimensions of 2.4 to 2.6 perform the more superior structural evolution during loading, including crack distribution, force chain structure, and particle fragment. It indicates that the optimization of the PSD of aggregates has unprecedented potential for improving the structure and strength of CWRB from the level of mesoscopic structural evolution.

**Availability of data and materials** The datasets used and/or analyzed during the current study are available from the corresponding author on reasonable request.

**Authors' contributions** J.Y. Wu and Q. Yin conceived and designed the experiments. J.Y. Wu, Q. Yin, Y. Gao, and B. Meng performed the experiments. J.Y. Wu, Q. Yin, and H.W. Jing analyzed the data. J.Y. Wu, Q. Yin, and H.W. Jing wrote the paper.

**Funding** This work was supported by the National Natural Science Foundation of China (52004272, 51734009, 51904290), Natural Science Foundation of Jiangsu Province, China (BK20200660, BK20180663), Engineering Research Center of Development and Management for Low to Ultra-Low Permeability Oil & Gas Reservoirs in West China, Ministry of Education, Xi'an Shiyou University (KFJJ-XB-2020-6), China Postdoctoral Science Foundation (2019M661987).

## Compliance with ethical standards

**Conflict of interest** The authors declare that they have no conflict of interest.

**Ethical approval** Not applicable.

**Consent to participate** Not applicable.

**Consent to publish** Not applicable.

## References

- ASTM Standard C192/C192M-13a (2013) Standard practice for making and curing concrete test specimens in the lab. Annual Book of ASTM Standards, West Conshohocken. Available online: [https://doi.org/10.1520/C0192\\_C0192M-13A](https://doi.org/10.1520/C0192_C0192M-13A)
- ASTM Standard C39/C39M-15a (2015) Standard test method for compressive strength of cylindrical concrete specimens. Annual Book of ASTM Standards, West Conshohocken. Available online: [https://doi.org/10.1520/C0039\\_C0039M-15A](https://doi.org/10.1520/C0039_C0039M-15A)
- Assi LN, Deaver EE, Ziehl P (2018) Effect of source and particle size distribution on the mechanical and microstructural properties of fly ash-based geopolymer concrete. *Constr Build Mater* 167:372–380
- Belem T, Benzaazoua M (2008) Design and application of underground mine paste backfill technology. *Geotech Geol Eng* 26(2):175–175
- Benzaazoua M, Belem T, Bussière B (2002) Chemical factors that influence the performance of mine sulphidic paste backfill. *Cem Concr Res* 32(7):1133–1144
- Bian ZF, Miao XX, Lei SG, Chen SE, Wang WF, Struthers S (2012) The challenges of reusing mining and mineral-processing wastes. *Science*. 337(6095):702–703
- Cao S, Song WD, Yilmaz E (2018) Influence of structural factors on uniaxial compressive strength of cemented tailings backfill. *Constr Build Mater* 174:190–201
- Cao S, Yilmaz E, Song WD (2019) Fiber type effect on strength, toughness and microstructure of early age cemented tailings backfill. *Constr Build Mater* 223:44–54
- Cao S, Xue GL, Yilmaz E, Yin ZY, Yang FD (2021) Utilizing concrete pillars as an environmental mining practice in underground mines. *J Clean Prod* 278:123433
- Chen QS, Zhang QL, Qi CC, Fourie A, Xiao CC (2018) Recycling phosphogypsum and construction demolition waste for cemented paste backfill and its environmental impact. *J Clean Prod* 186:418–429
- Cihangir F, Ercikdi B, Kesimal A, Turan A, Deveci H (2012) Utilisation of alkali-activated blast furnace slag in paste backfill of high-sulphide mill tailings: effect of binder type and dosage. *Miner Eng* 30(4):33–43
- Cui L, Fall M (2016) Mechanical and thermal properties of cemented tailings materials at early ages: influence of initial temperature, curing stress and drainage conditions. *Constr Build Mater* 125:553–563
- Deng DQ, Liu L, Yao ZL, Song K, Lao DZ (2017) A practice of ultra-fine tailings disposal as filling material in a gold mine. *J Environ Manag* 196:100–109
- Ercikdi B, Cihangir F, Kesimal A, Deveci H, Alp İ (2009a) Utilization of industrial waste products as pozzolanic material in cemented paste backfill of high sulphide mill tailings. *J Hazard Mater* 168(2–3): 848–856
- Ercikdi B, Kesimal A, Cihangir F, Deveci H, Alp İ (2009b) Cemented paste backfill of sulphide-rich tailings: importance of binder type and dosage. *Cement Concrete Comp* 31(4):268–274
- Ercikdi B, Yilmaz T, Külekci G (2014) Strength and ultrasonic properties of cemented paste backfill. *Ultrasonics*. 54(1):195–204
- Fall M, Benzaazoua M, Ouellet S (2005) Experimental characterization of the influence of tailings fineness and density on the quality of cemented paste backfill. *Miner Eng* 18(1):41–44

- Huang YH, Yang SQ, Tian WL (2019) Crack coalescence behavior of sandstone specimen containing two pre-existing flaws under different confining pressures. *Theor Appl Fract Mec* 99:118–130
- Jiang HQ, Yi HS, Yilmaz E, Liu SW, Qiu JP (2020) Ultrasonic evaluation of strength properties of cemented paste backfill: effects of mineral admixture and curing temperature. *Ultrasonics*. 100(1):105983
- Ke X, Zhou X, Wang XS, Wang T, Hou HB, Zhou M (2016) Effect of tailings fineness on the pore structure development of cemented paste backfill. *Constr Build Mater* 126:345–350
- Li M, Zhang JX, Li AL, Zhou N (2020) Reutilisation of coal gangue and fly ash as underground backfill materials for surface subsidence control. *J Clean Prod* 254:120113
- Li XB, Du J, Gao L, He SY, He SY, Gan L, Sun C, Shi Y (2017) Immobilization of phosphogypsum for cemented paste backfill and its environmental effect. *J Clean Prod* 156:137–146
- Liu B, Gao YT, Jin AB, Xue W (2020) Influence of water loss on mechanical properties of superfine tailing-blast-furnace slag backfill. *Constr Build Mater* 246(6):118482
- Liu QS, Liu DF, Tian YC, Liu XY (2017) Numerical simulation of stress-strain behaviour of cemented paste backfill in triaxial compression. *Eng Geol* 231:165–175
- Liu RC, Li B, Jiang YJ, Yu LY (2018) A numerical approach for assessing effects of shear on equivalent permeability and nonlinear flow characteristics of 2-D fracture networks. *Adv Water Resour* 111:289–300
- Ma D, Duan HY, Liu JF, Li XB, Zhou ZL (2019a) The role of gangue on the mitigation of mining-induced hazards and environmental pollution: an experimental investigation. *Sci Total Environ* 664:636–448
- Ma D, Duan HY, Li XB, Li ZH, Zhou ZL, Li TB (2019b) Effects of seepage-induced erosion on nonlinear hydraulic properties of broken red sandstones. *Tunn Under Sp Tech* 91:102993
- Ma D, Duan HY, Liu WT, Ma XT, Tao M (2020) Water-sediment two-phase flow inrush hazard in rock fractures of overburden strata during coal mining. *Mine Water Environ* 39:308–319
- Ma D, Zhang JX, Duan HY, Huang YL, Li M, Sun Q, Zhou N (2021) Reutilization of gangue wastes in underground backfilling mining: Overburden aquifer protection. *Chemosphere* 264:128400
- Sari D, Pasamehmetoglu AG (2005) The effects of gradation and admixture on the pumice lightweight aggregate concrete. *Cem Concr Res* 35(5):936–942
- Sevim Ö, Demir İ (2019) Physical and permeability properties of cementitious mortars having fly ash with optimized particle size distribution. *Cement Concrete Comp* 96:266–273
- Shi XS, Zhao J (2020) Practical estimation of compression behavior of clayey/silty sands using equivalent void-ratio concept. *J Geotech Geoenviron* 146:04020046
- Sun Q, Tian S, Sun QW, Li B, Cai C, Xia YJ, Wei X, Mu QW (2019) Preparation and microstructure of fly ash geopolymer paste backfill material. *J Clean Prod* 225:376–390
- Tian WL, Yang SQ, Huang YH, Hu B (2020) Mechanical behavior of granite with different grain sizes after high-temperature treatment by particle flow simulation. *Rock Mech Rock Eng* 53:1791–1807
- Wu D, Zhang YL, Liu YC (2016) Mechanical performance and ultrasonic properties of cemented gangue backfill with admixture of fly ash. *Ultrasonics*. 64:89–96
- Wu JY, Feng MM, Mao XB, Xu JM, Zhang WL, Ni XY, Han GS (2018) Particle size distribution of aggregate effects on mechanical and structural properties of cemented rockfill: experiments and modeling. *Constr Build Mater* 193:295–311
- Wu JY, Feng MM, Ni XY, Mao XB, Chen ZQ, Han GS (2019) Aggregate gradation effects on dilatancy behavior and acoustic characteristic of cemented rockfill. *Ultrasonics*. 92(2):79–92
- Wu JY, Jing HW, Yin Q, Meng B, Han GS (2020) Strength and ultrasonic properties of cemented waste rock backfill considering confining pressure, dosage and particle size effects. *Constr Build Mater* 242:118132
- Yilmaz E, Belem T, Bussi ere B, Mbonimpa M, Benzaazoua M (2015) Curing time effect on consolidation behaviour of cemented paste backfill containing different cement types and contents. *Constr Build Mater* 75(75):99–111
- Yilmaz E (2018) Stope depth effect on field behaviour and performance of cemented paste backfills. *Int J Min Reclam Environ* 32(4):273–296
- Zuo JP, Hong ZJ, Xiong ZQ, Wang C, Song HQ (2018) Influence of different W/C on the performances and hydration progress of dual liquid high water backfilling material. *Constr Build Mater* 190:910–917

**Publisher's note** Springer Nature remains neutral with regard to jurisdictional claims in published maps and institutional affiliations.